Target-oriented joint inversion of incomplete time-lapse seismic data sets

Gboyega Ayeni and Biondo Biondi

ABSTRACT

We propose a joint inversion method, based on linear least-squares wave-equation inversion, for imaging incomplete time-lapse seismic data sets. Such data sets can arise from presence of production facilities or intentional *sparse sampling*. These data sets generate undesirable artifacts that degrade the quality of time-lapse seismic images, making them unreliable indicators of production-related changes in reservoir properties. To solve this problem, we pose time-lapse imaging as a joint linear inverse problem that utilizes concatenations of target-oriented approximations to the least-squares imaging Hessian. Using a subset of the 2D Marmousi model, we show that the proposed method gives reliable time-lapse seismic images from incomplete seismic data sets.

INTRODUCTION

There is a wide range of published work on the most important aspects of time-lapse seismic imaging. Some of these works include studies of seismic properties of reservoir fluids (Batzle and Wang, 1992), processing and practical applications (Rickett and Lumley, 2001; Calvert, 2005), and successful case studies (Lefeuvre et al., 2003; Whitcombe et al., 2004; Zou et al., 2006). Because of many successful applications, time-lapse seismic imaging is now an integral part of many reservoir management projects.

A recurring problem in many field time-lapse seismic applications is the presence (and sometimes changing locations) of production and development facilities. Such facilities prevent perfect geometry repetition for different surveys and can pose a major challenge when they are directly located above producing reservoirs. In order to circumvent this problem, it is common practice to *undershoot* the facilities using two or more boats. However, the *undershoot* approach does not work in all situations, mainly because the shot/receiver offset distributions cannot be perfectly matched.

Incomplete time-lapse seismic data sets also arise from intentional subsampling of seismic data sets. Such regularly (Calvert and Wills, 2003; Smit et al., 2006) or randomly (Arogunmati and Harris, 2007) subsampled data sets reduce the overall acquisition cost requirement for multiple seismic surveys. Successful field application of regularly sub-sampled time-lapse data sets has been demonstrated by previous

authors (Calvert and Wills, 2003; Smit et al., 2006). Although regularly sampled data sets removes unnecessary redundancy in time-lapse data sets and can sufficiently sample low frequency spatial changes in reservoir properties, high frequency changes will likely not be captured. Acquiring seismic data sets randomly can ensure that all parts of the evolving reservoir are sampled, but with different densities/folds for any given survey. Randomly sampled data sets can be interpolated and then processed as full-volume data sets (Arogunmati and Harris, 2007), or they can be directly used to reconstruct the reservoir using compressive sampling (Candes and Romberg, 2007; Candes and Wakin, 2008) principles.

We propose a joint inversion method, based on an iterative least-squares inversion of the linearized wave-equation, for direct imaging of randomly sparse/incomplete time-lapse seismic data sets. The method utilizes a system of non-stationary filters derived from an explicitly computed target-oriented approximation (Valenciano, 2008) to the linear least-squares wave-equation Hessian. A joint inversion scheme enables incorporation of structural constraints (e.g., reservoir location and geometry) and temporal constraints (e.g., smooth temporal changes) in time-lapse image estimation. The proposed method, regularized joint inversion of multiple images (RJMI), and related methods have been applied to other time-lapse seismic imaging problems (Ajo-Franklin et al., 2005; Ayeni and Biondi, 2008; Ayeni et al., 2009).

We assume that the background baseline velocity model is known and that it changes slowly between surveys. Large velocity changes and geomechanical shifts can be handled by including an event alignment step prior to or during inversion. Integration of geomechanical shifts into the joint inversion formulation is ongoing and will be discussed elsewhere. A solution of the joint inversion problem using a robust (reweighted least-squares) L1-framework is also ongoing.

In this paper, using matrix-vector notations, we first review linear wave-equation modeling, iterative least-squares migration/inversion, and the RJMI method. Then, using a subset of the 2D Marmousi model (Versteeg, 1994), we show that RJMI gives good quality time-lapse images from incomplete seismic data sets.

Least-squares inversion of time-lapse seismic data sets

Within limits of the Born approximation of the linearized acoustic wave equation, synthetic seismic data set $\mathbf{d}$ is obtained by the action of a modeling operator $\mathbf{L}$ on the earth reflectivity $\mathbf{m}$:

$$\mathbf{d} = \mathbf{L}\mathbf{m}. \tag{1}$$

Given two data sets (baseline and monitor), acquired over an evolving earth model at times $\mathbf{0}$ and $\mathbf{1}$ respectively, we can write

$$\begin{aligned} \mathbf{d}_0 &= \mathbf{L}_0\mathbf{m}_0, \\ \mathbf{d}_1 &= \mathbf{L}_1\mathbf{m}_1, \end{aligned} \tag{2}$$

where $\mathbf{m}_0$ and $\mathbf{m}_1$ are the baseline and monitor reflectivities, and $\mathbf{d}_0$ and $\mathbf{d}_1$ are the data sets modeled by $\mathbf{L}_0$ and $\mathbf{L}_1$.

Applying the adjoint operators $\bar{\mathbf{L}}_0^T$ and $\bar{\mathbf{L}}_1^T$ to $\mathbf{d}_0$ and $\mathbf{d}_1$ respectively, we obtain the migrated baseline $\tilde{\mathbf{m}}_0$ and monitor $\tilde{\mathbf{m}}_1$ images:

$$\begin{aligned} \tilde{\mathbf{m}}_0 &= \bar{\mathbf{L}}_0^T \mathbf{d}_0, \\ \tilde{\mathbf{m}}_1 &= \bar{\mathbf{L}}_1^T \mathbf{d}_1, \end{aligned} \tag{3}$$

where $\bar{\mathbf{L}}_i^T$ denotes conjugate transpose of $\mathbf{L}_i$. The *raw* time-lapse image $\Delta\tilde{\mathbf{m}}$ is the difference between the migrated images:

$$\Delta\tilde{\mathbf{m}} = \tilde{\mathbf{m}}_1 - \tilde{\mathbf{m}}_0. \tag{4}$$

Because incomplete seismic data sets leads to high non-repeatability, $\tilde{\mathbf{m}}_\mathbf{0}$ and $\tilde{\mathbf{m}}_\mathbf{1}$ must be *cross-equalized* before $\Delta\tilde{\mathbf{m}}$ is computed. The high level of non-repeatability makes it difficult to adapt existing cross-equalization methods (Rickett and Lumley, 2001; Calvert, 2005; Hall, 2006) to randomly sampled time-lapse seismic data sets. The RJMI method takes the data acquisition geometry and sampling into account and hence can correct for the non-repeatability of the data sets.

We define two quadratic cost functions for the modeling experiments (equation 2):

$$\begin{aligned} S(\mathbf{m_0}) &= \|\mathbf{L}_0\mathbf{m}_0 - \mathbf{d}_0\|_2^2, \\ S(\mathbf{m_1}) &= \|\mathbf{L}_1\mathbf{m}_1 - \mathbf{d}_1\|_2^2, \end{aligned} \tag{5}$$

which, when minimized, give the least-squares solutions $\hat{\mathbf{m}}_\mathbf{0}$ and $\hat{\mathbf{m}}_\mathbf{1}$, where

$$\begin{aligned} \hat{\mathbf{m}}_0 &= (\bar{\mathbf{L}}_0^T\mathbf{L}_0)^\dagger \bar{\mathbf{L}}_0^T \mathbf{d}_0, \\ \hat{\mathbf{m}}_1 &= (\bar{\mathbf{L}}_1^T\mathbf{L}_1)^\dagger \bar{\mathbf{L}}_1^T \mathbf{d}_1, \end{aligned} \tag{6}$$

and $(\cdot)^\dagger$ denotes approximate inverse.

Because seismic inversion is ill-posed, model regularization is often required to ensure stability and convergence to a geologically consistent solution. For many seismic monitoring objectives, the known geology and reservoir architecture provide useful regularization information. Including baseline and monitor regularization operators ($\mathbf{R}_0$ and $\mathbf{R}_1$ respectively) in the cost functions gives

$$\begin{aligned} S(\mathbf{m_0}) &= \|\mathbf{L}_0\mathbf{m}_0 - \mathbf{d}_0\|_2^2 + \epsilon_0^2\|\mathbf{R}_0\mathbf{m}_0\|^2, \\ S(\mathbf{m_1}) &= \|\mathbf{L}_1\mathbf{m}_1 - \mathbf{d}_1\|_2^2 + \epsilon_1^2\|\mathbf{R}_1\mathbf{m}_1\|^2, \end{aligned} \tag{7}$$

which have the solutions

$$\begin{aligned} \hat{\mathbf{m}}_0 &= (\bar{\mathbf{L}}_0^T\mathbf{L}_0 + \epsilon_0^2\mathbf{R}_0^T\mathbf{R}_0)^\dagger \bar{\mathbf{L}}_0^T \mathbf{d}_0, \\ \hat{\mathbf{m}}_1 &= (\bar{\mathbf{L}}_1^T\mathbf{L}_1 + \epsilon_1^2\mathbf{R}_1^T\mathbf{R}_1)^\dagger \bar{\mathbf{L}}_1^T \mathbf{d}_1. \end{aligned} \tag{8}$$

where ϵ_i is a regularization parameter that determines the strength of the regularization relative to the data fitting goal. Although there is a wide range of suggested

methods for selecting ϵ_i, in most practical applications, the final choice of the parameter is subjective. Unless otherwise stated, we use a fixed, heuristically determined, data-dependent regularization parameter given by

$$\epsilon_i = \frac{max|\mathbf{d}_i|}{50}. \tag{9}$$

Estimating $\hat{\mathbf{m}}_\mathbf{0}$ or $\hat{\mathbf{m}}_\mathbf{1}$ by minimizing equation 7 is the so-called *data-space* least-squares migration/inversion method (Clapp, 2005).

Substituting equation 3 into equation 8, and re-arranging the terms, we get

$$\begin{aligned} [\mathbf{H}_0 + \mathbf{R}_{00}]\,\hat{\mathbf{m}}_0 &= \tilde{\mathbf{m}}_0, \\ [\mathbf{H}_1 + \mathbf{R}_{11}]\,\hat{\mathbf{m}}_1 &= \tilde{\mathbf{m}}_1, \end{aligned} \tag{10}$$

where $\mathbf{H}_i = \bar{\mathbf{L}}_i^T\mathbf{L}_i$ is the Hessian, and $\mathbf{R}_{ii} = \epsilon_i^2\mathbf{R}_i^T\mathbf{R}_i$ is the regularization term. Equation 10 can be solved using iterative inverse filtering leading to the so-called *model-space* least-squares migration/inversion method (Valenciano, 2008). We summarize linearized (Born) wave-equation data modeling and the least-squares Hessian derivation in Appendix *A*. Throughout this paper, our discussion of the Hessian refers to its target-oriented approximation defined in equation A-5.

An inverted time-lapse image, $\Delta\hat{\mathbf{m}}$, can be obtained as the difference between the two images, $\hat{\mathbf{m}}_0$ and $\hat{\mathbf{m}}_1$:

$$\Delta\hat{\mathbf{m}} = \hat{\mathbf{m}}_1 - \hat{\mathbf{m}}_0. \tag{11}$$

In this paper, we refer to the method of computing the time-lapse image using equation 11 as *separate inversion*.

Joint inversion of multiple images

In order to solve a single joint inversion problem in which the baseline and monitor images are simultaneously estimated, we combine the two expressions in equation 2 to get

$$\begin{bmatrix} \mathbf{d}_0 \\ \mathbf{d}_1 \end{bmatrix} = \begin{bmatrix} \mathbf{L}_0 & \mathbf{0} \\ \mathbf{0} & \mathbf{L}_1 \end{bmatrix} \begin{bmatrix} \mathbf{m}_0 \\ \mathbf{m}_1 \end{bmatrix}, \tag{12}$$

which can be solved by minimizing the cost function

$$S(\mathbf{m_0}, \mathbf{m_1}) = \left|\left| \begin{bmatrix} \mathbf{L}_0 & \mathbf{0} \\ \mathbf{0} & \mathbf{L}_1 \end{bmatrix} \begin{bmatrix} \mathbf{m}_0 \\ \mathbf{m}_1 \end{bmatrix} - \begin{bmatrix} \mathbf{d}_0 \\ \mathbf{d}_1 \end{bmatrix} \right|\right|_2^2, \tag{13}$$

to obtain the solution

$$\begin{bmatrix} \hat{\mathbf{m}}_0 \\ \hat{\mathbf{m}}_1 \end{bmatrix} = \begin{bmatrix} \bar{\mathbf{L}}_0^T\mathbf{L}_0 & \mathbf{0} \\ \mathbf{0} & \bar{\mathbf{L}}_1^T\mathbf{L}_1 \end{bmatrix}^\dagger \begin{bmatrix} \bar{\mathbf{L}}_0^T & \mathbf{0} \\ \mathbf{0} & \bar{\mathbf{L}}_1^T \end{bmatrix} \begin{bmatrix} \mathbf{d}_0 \\ \mathbf{d}_1 \end{bmatrix}, \tag{14}$$

where † is the pseudo refers to the pseudo-inverse.

The RJMI method differs from separate inversion, because it enables inclusion of both spatial regularization (as in separate inversion) and temporal regularization (e.g., Tikhonov) so that the cost function becomes

$$S(\mathbf{m_0},\mathbf{m_1}) = \left|\left|\begin{bmatrix} \mathbf{L}_0 & \mathbf{0} \\ \mathbf{0} & \mathbf{L}_1 \end{bmatrix}\begin{bmatrix} \mathbf{m}_0 \\ \mathbf{m}_1 \end{bmatrix} - \begin{bmatrix} \mathbf{d}_0 \\ \mathbf{d}_1 \end{bmatrix}\right|\right|^2 + \\ \left|\left|\begin{bmatrix} \epsilon_0\mathbf{R}_0 & \mathbf{0} \\ \mathbf{0} & \epsilon_1\mathbf{R}_1 \end{bmatrix}\begin{bmatrix} \mathbf{m}_0 \\ \mathbf{m}_1 \end{bmatrix}\right|\right|^2 + \left|\left|\begin{bmatrix} -\zeta_0\mathbf{\Lambda_0} & \zeta_1\mathbf{\Lambda_1} \end{bmatrix}\begin{bmatrix} \mathbf{m}_0 \\ \mathbf{m}_1 \end{bmatrix}\right|\right|^2, \tag{15}$$

where $\mathbf{\Lambda_i}$ is the temporal regularization, and ζ_i is a relative temporal regularization parameter that determines the strength of the temporal constraint. Similar formulations have been applied to seismic tomography (Ajo-Franklin et al., 2005) and medical imaging problems (Zhang et al., 2005). However, for our problem, a direct minimization of equation 15 with an iterative solver is computationally expensive:

$$cost \propto 2 \times N_{surv} \times N_{iter} \times C_{mig}, \tag{16}$$

where N_{surv} is the number of data sets, N_{iter} is the number of iterations, and C_{mig} is the cost of on migration. Although it is possible to reduce the computational cost by encoding the data sets (Ayeni et al., 2009), conventional single-record shot-profile implementation is too expensive for practical applications. Because several iterations are usually required to reach a useful solution, and because inversion is usually repeated several times to fine-tune parameters, the overall cost of this scheme makes it impractical. One advantage of the RJMI method is that modifications can be made to inversion parameters and the inversion repeated at several orders of magnitude more cheaply than iterative least-squares *data-space* migration/inversion. This cost reduction comes because the migration and modeling (demigration) operations are replaced by a single sparse-matrix convolution.

Minimizing equation 15 leads to the solutions $\hat{\mathbf{m}}_0$ and $\hat{\mathbf{m}}_1$:

$$\begin{bmatrix} \hat{\mathbf{m}}_0 \\ \hat{\mathbf{m}}_1 \end{bmatrix} = \left(\begin{bmatrix} \bar{\mathbf{L}}_0^T\mathbf{L}_0 & \mathbf{0} \\ \mathbf{0} & \bar{\mathbf{L}}_1^T\mathbf{L}_1 \end{bmatrix} + \begin{bmatrix} \mathbf{R}_0^T\mathbf{R}_0 & \mathbf{0} \\ \mathbf{0} & \mathbf{R}_1^T\mathbf{R}_1 \end{bmatrix} + \begin{bmatrix} \mathbf{\Lambda_0'^T\Lambda_0} & -\mathbf{\Lambda_0'^T\Lambda_1} \\ -\mathbf{\Lambda_1'^T\Lambda_0} & \mathbf{\Lambda_1'^T\Lambda_1} \end{bmatrix}\right)^{\dagger} \begin{bmatrix} \tilde{\mathbf{m}}_0 \\ \tilde{\mathbf{m}}_1 \end{bmatrix}, \tag{17}$$

which can be obtained via iterative recursive filtering:

$$\left(\begin{bmatrix} \mathbf{H}_0 & \mathbf{0} \\ \mathbf{0} & \mathbf{H}_1 \end{bmatrix} + \begin{bmatrix} \mathbf{R}_{00} & \mathbf{0} \\ \mathbf{0} & \mathbf{R}_{11} \end{bmatrix} + \begin{bmatrix} \mathbf{\Lambda_{00}} & -\mathbf{\Lambda_{01}} \\ -\mathbf{\Lambda_{10}} & \mathbf{\Lambda_{11}} \end{bmatrix}\right) \begin{bmatrix} \hat{\mathbf{m}}_0 \\ \hat{\mathbf{m}}_1 \end{bmatrix} = \begin{bmatrix} \tilde{\mathbf{m}}_0 \\ \tilde{\mathbf{m}}_1 \end{bmatrix}, \tag{18}$$

where

$$\begin{aligned} \mathbf{R_{ij}} &= \epsilon_\mathbf{i}\mathbf{R'}_\mathbf{i}\epsilon_\mathbf{j}\mathbf{R_j} \\ \Lambda_\mathbf{ij} &= \zeta_\mathbf{i}\mathbf{\Lambda'}_\mathbf{i}\zeta_\mathbf{j}\mathbf{\Lambda_j} \end{aligned}. \tag{19}$$

Following the same procedure, equation 18 can be directly extended to an arbitrary number of surveys (Ayeni and Biondi, 2008). Note that it is unnecessary to explicitly form the Hessian operators in equations 18 because they are composed of

simple combinations of $\mathbf{H_0}$ to $\mathbf{H_N}$ for N surveys. Also, $\mathbf{R_{ij}}$ and $\Lambda_{\mathbf{ij}}$ are not explicitly computed, but instead, the regularization operators $\mathbf{R_i}$ and $\mathbf{\Lambda_i}$ (and their adjoints) are applied at each inversion step. Depending on the problem size, computational domain and available a priori information, the spatial and temporal regularization operators can be applied over several dimensions (e.g., stacked-image, subsurface offset, subsurface scattering-angles, etc.). We have implemented these operators for any arbitrary number of surveys using sparse convolution operators. Unless otherwise stated, equation 19 is solved with a conjugate gradient algorithm.

NUMERICAL EXAMPLES

We consider two incomplete synthetic time-lapse seismic examples aimed at imaging seismic amplitude changes using incomplete time-lapse seismic data sets. Both examples are based on a modified section of the Marmousi model (Figure 1) with the target reservoir located at a shallower depth than the original Marmousi reservoir. In both examples, we neglect geomechanical changes above the reservoir.

In both cases, the baseline data set consists of 111 surface shots spaced at 80 m and 551 receivers spaced at 16 m. In the first example, the monitor data sets were modeled with gaps in data created by obstructions along the survey line (Figure 2). The monitor data sets in the second example consist of randomly sampled shot and receiver axis (Figure 3). We avoid a multiple attenuation requirement by using a Born single-scattering modeling algorithm. We migrated the data sets with the oneway wave-equation, using 184 frequencies and computed the target-oriented Hessian with 72 frequencies.

We compare the results from migration, normalization with the Hessian diagonal, separate, and joint inversion for the target area in Figure 1. Normalization with the Hessian diagonal is one implementation of the so-called true-amplitude migration (Gray, 1997). In both examples, the same spatial regularization parameters were used for the separately and jointly inverted results. Where applicable, the regularization operators are Laplacian in x-direction and first-order gradient in time.

Undershoot problem

This example demonstrates the *undershoot* problem , where obstructions caused by latter development facilities prevent complete recording of monitor data sets. Here, we consider an obstruction with changes in its location and size (Figure 2) for the three monitor data sets. This is a common scenario in seismic monitoring applications where the construction, addition and alteration of production facilities create obstructions. In each monitor survey, neither shot nor receivers were located within the undershoot area (Figure 2).

Migrated images of the target area for all four data sets are shown in Figure 4(a),

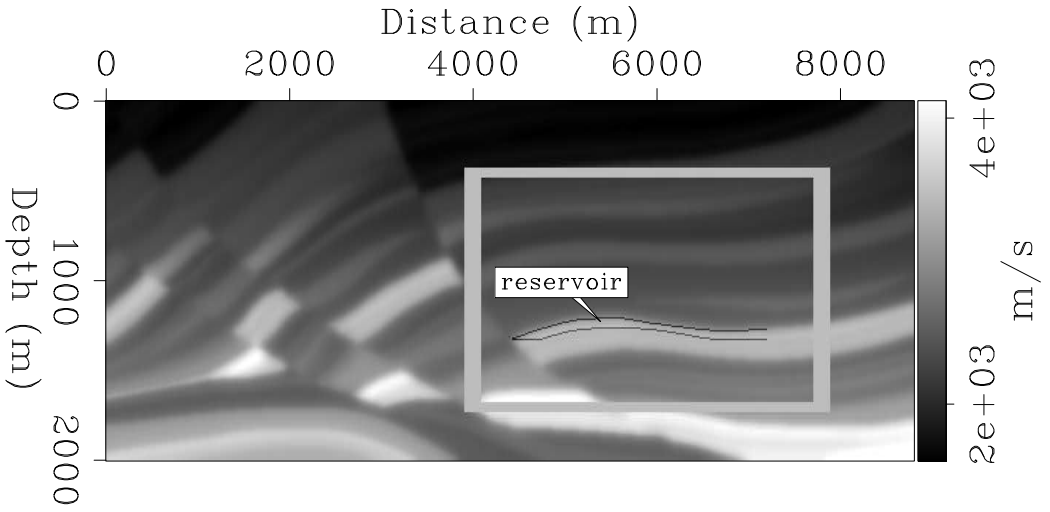

Figure 1: Modified section of the Marmousi velocity model showing the reservoir location. The gray box shows the target area.[**ER**]

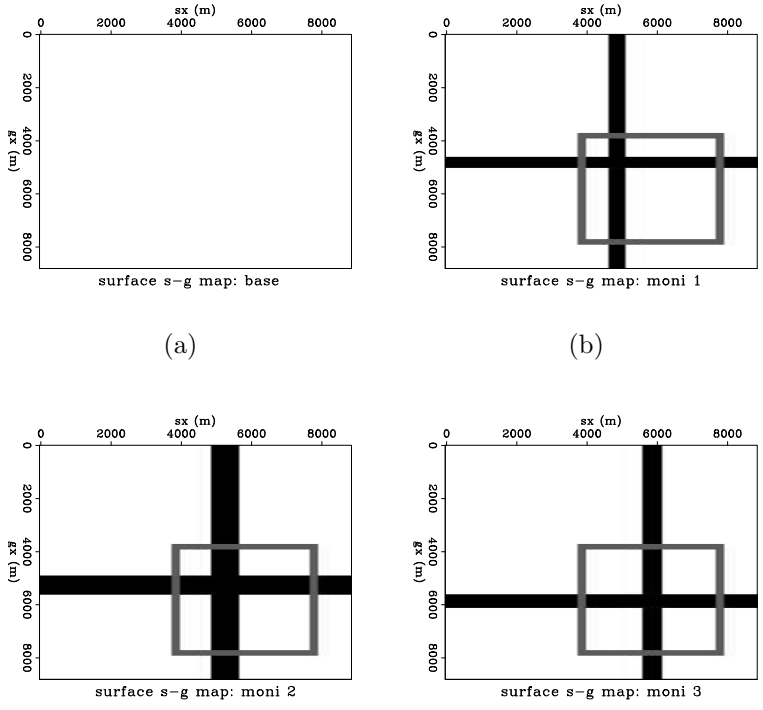

Figure 2: Surface shot-geophone coverage maps for the (a) baseline and (b)-(d) monitor surveys. White indicates locations with shot-receiver coverage whereas black gaps indicate the undershoot positions. The gray box indicates the surface location of the target area in both this Figure and also in Figure 3.[**ER**]

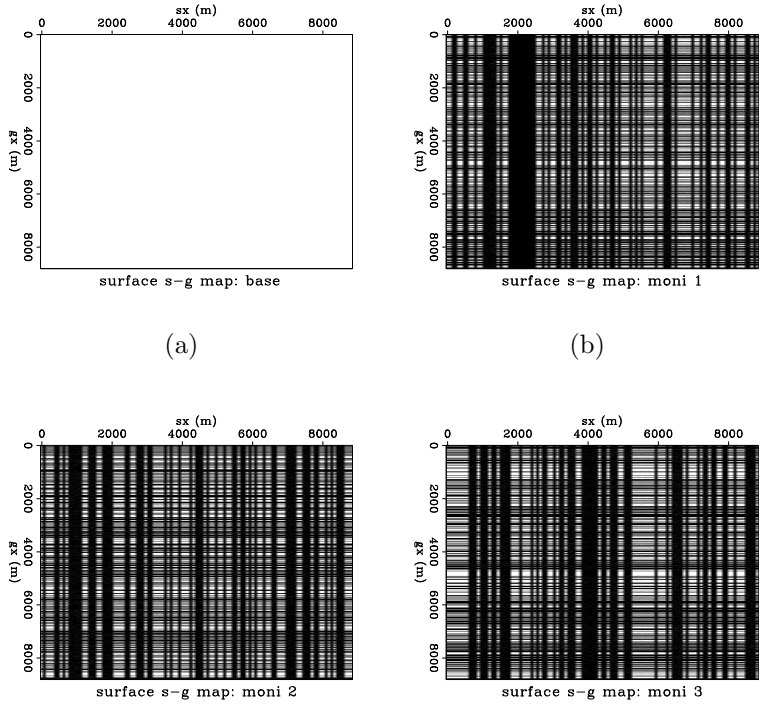

(a) (b)

(c) (d)

Figure 3: Surface shot-geophone coverage maps for the (a) baseline and (b)-(d) monitor surveys. White indicates locations with shot-receiver coverage whereas black indicates no coverage.[**ER**]

and the corresponding Hessian diagonals (so-called *illumination*) in Figures 4(b). Figure 4(c) shows the cumulative time-lapse image of the target area obtained from the full data sets, and Figure 4(d) shows the illumination ratio between monitor and baseline data sets. The migrated, normalized, separately and jointly inverted time-lapse images are shown in Figure 5. Note that time-lapse images obtained from joint inversion [Figure 5(d)] contain fewer artifacts relative to those from migration, normalization and separate invertion [Figures 5(a) to 5(c)].

Sparse data problem

This example demonstrates a particular sparse time-lapse seismic monitoring problem (Arogunmati and Harris, 2007), where sparse randomly-sampled monitor data sets are acquired at a fraction of the cost of the full survey. Here, we consider a full baseline data set and three randomly sampled monitor surveys each constituting only 25 percent—at 50 per cent source and receiver sampling—of the full data set (Figure 3).

Migrated images of the target area are shown in Figure 6(a), and the corresponding Hessian diagonals in Figure 6(b). Figure 6(c) shows the cumulative time-lapse images of the target area obtained from the full data sets, and Figure 6(d) the illumination ratio between monitor and baseline data sets. The migrated, normalized, separately and jointly inverted time-lapse images are shown in Figure 7. Note that the migrated and normalized time-lapse images [Figures 7(a) and 7(b)] show no resemblance to the full data results [Figure 6(c)]. Also, note that time-lapse images obtained from joint inversion [Figure 7(d)] contain fewer artifacts than those from separate invertion [Figure 7(c)].

DISCUSSION

From the numerical examples, we see that incomplete time-lapse seismic data-sets degrade time-lapse images [Figures 5(a) and 7(a)]. This image degradation is expected because the migration does not compensate for the resulting geometry (and hence illumination) differences in the migrated images (Figures 4(a) and 6(a)).

Normalization with the Hessian diagonal is insufficient to adequately attenuate undershoot artifacts [Figure 5(b)] and is markedly insufficient in the sparse data example [Figure 7(b)]. Although it is possible that specialized regularization methods can attenuate some of these artifacts, we suspect that most conventional cross-equalization methods will be inadequate.

Although separate inversion improves the quality of the time-lapse images relative to migration and normalization, several relatively high-amplitude artifacts persist [Figures 5(c) and 7(c)]. The high-amplitude artifacts in Figures 5(c) and 7(c) result from a mismatch of residual artifacts from the independent inversion of the data sets.

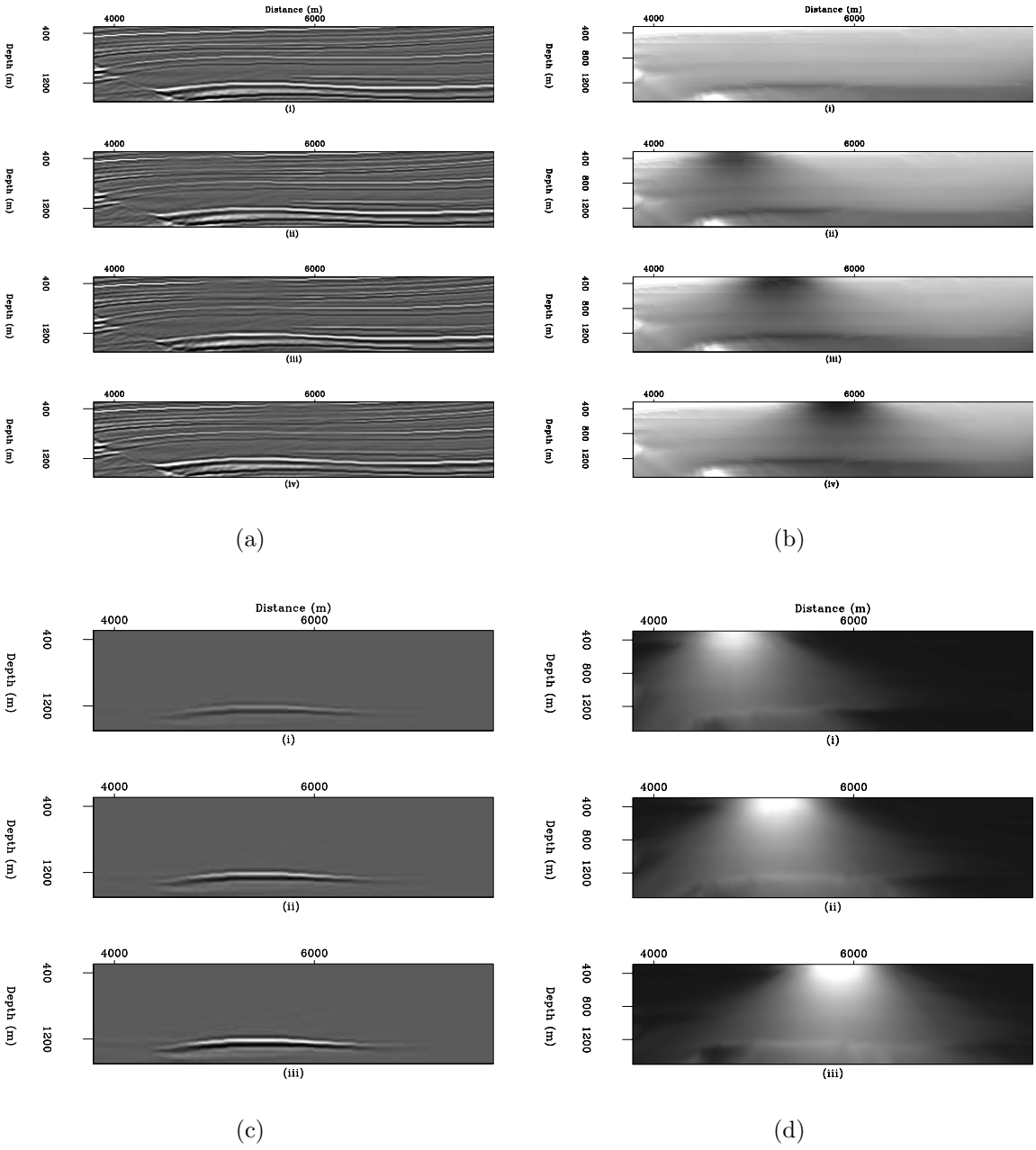

Figure 4: (a) Migrated (i) baseline and (ii)-(iv) monitor images. (b) Hessian diagonal corresponding to images in (a). (c) Cumulative time-lapse images from full baseline and monitor shot-receiver coverage [Figure 2(a)]. (d) Illumination-ratio for each monitor survey [Figures b(ii)-(iv)] relative to the baseline [Figure b(i)].[**CR**]

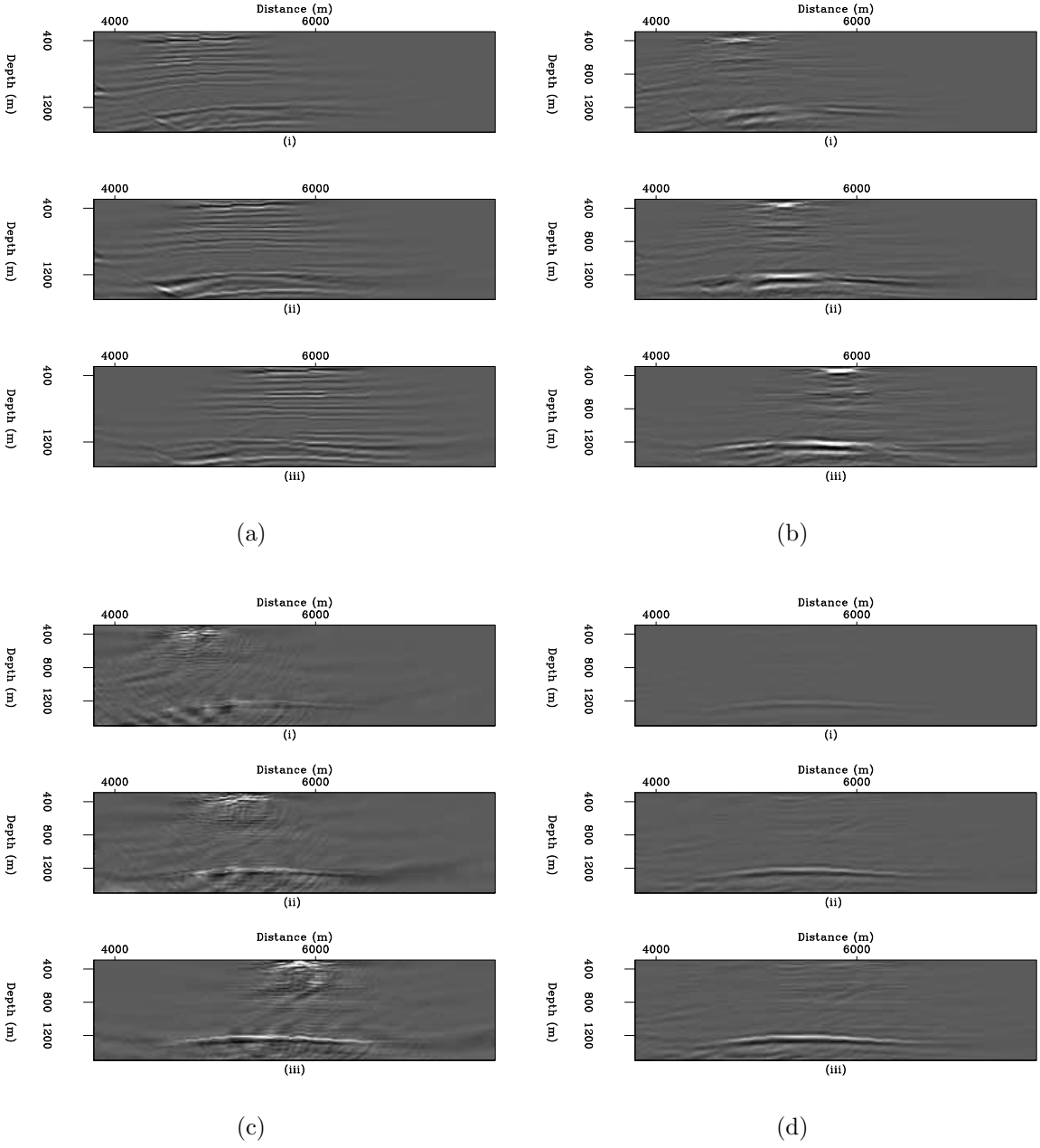

Figure 5: Cumulative time-lapse images at four production stages (with increasing production from top to bottom) obtained from (a) migration, (b) Hessian-diagonal illumination correction, (c) separate inversion, and (d) RJMI. Compare these results to those from the full data sets [Figure 4(c)].[**CR**]

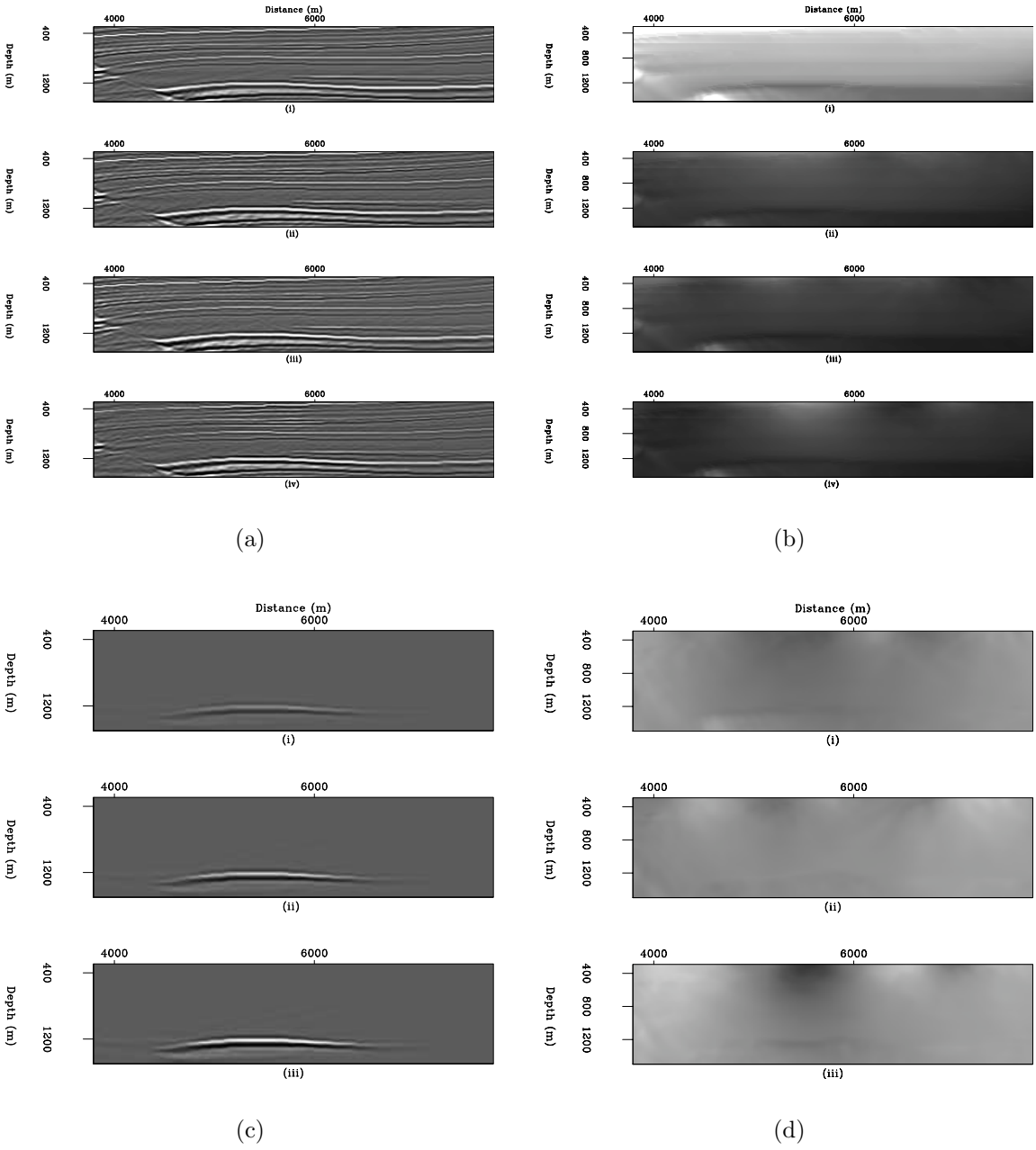

Figure 6: (a) Migrated (i) baseline and (ii)-(iv) monitor images. (b) Hessian diagonal corresponding to images in (a). (c) Cumulative time-lapse images from full baseline and monitor shot-receiver coverage [Figure 2(a)]. (d) Illumination-ratio for each monitor survey [Figures b(ii)-(iv)] relative to the baseline [Figure b(i)].[**CR**]

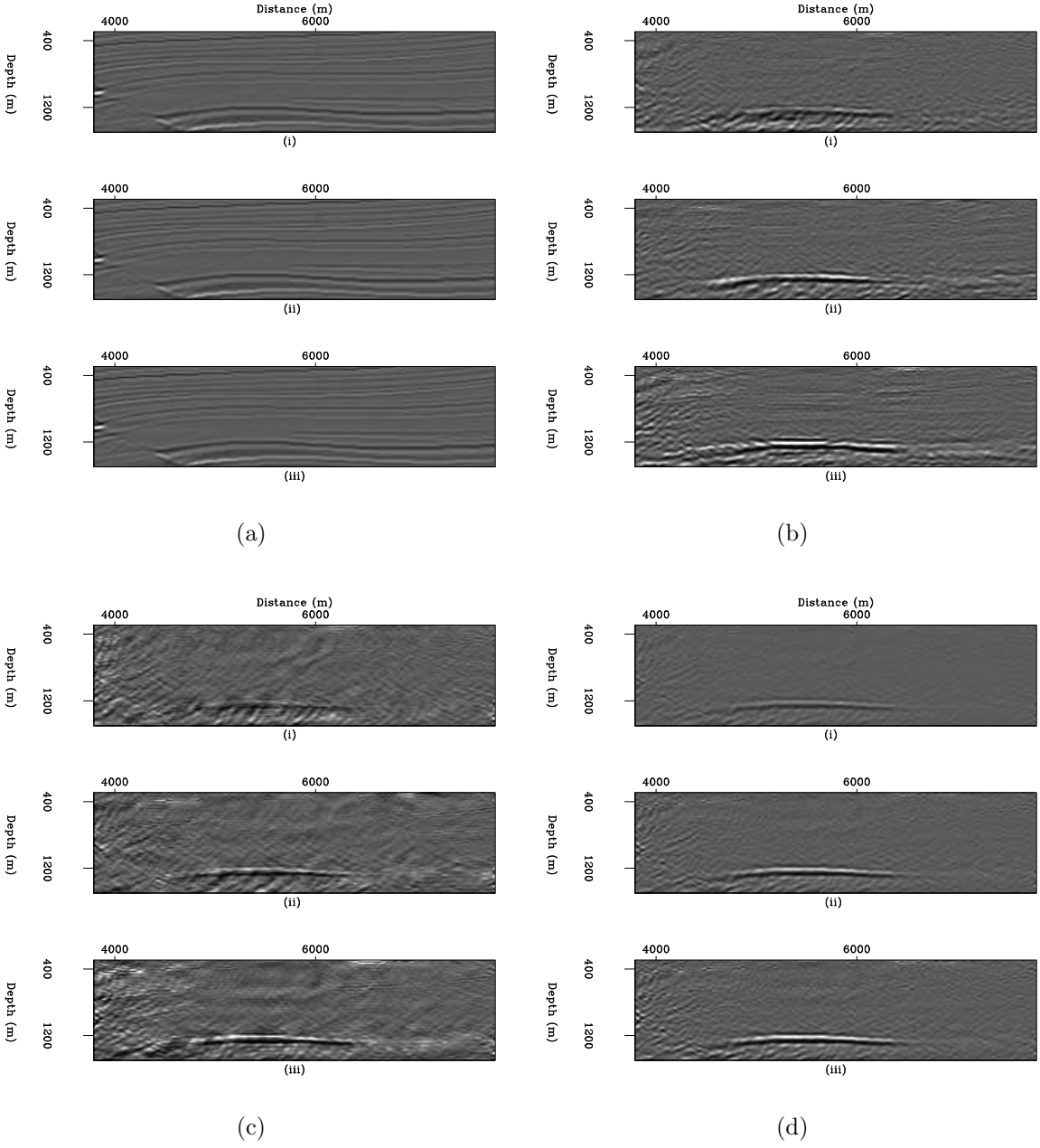

Figure 7: Cumulative time-lapse images at four production stages (with increasing production from top to bottom) obtained from (a) migration, (b) Hessian-diagonal illumination correction, (c) separate inversion, and (d) RJMI. Compare these results to those from the full data sets [Figure 6(c)].[**CR**]

Recall that the target-oriented approximation captures limited information contained in a poorly-conditioned full Hessian matrix. Although the spatial regularization improves the conditioning of the problem, residual artifacts in final results from each inversion differ and do not tend to cancel out.

In the undershoot example, joint inversion of all the data sets (using the RJMI method), improves the time-lapse image quality substantially [Figure 7(d)]. The improvement in the time-lapse images obtained via RJMI vs. separate inversion result from an inclusion of temporal constraints in the RJMI inversion. There is also significant reduction in artifacts in the RJMI sparse data results [Figure 7(d)] relative to separate inversion [Figure 7(c)]. However, in this sparse data example, there are still several residual artifacts in joint inversion results. These artifacts can be further attenuated using stronger regularization (at the cost of the data-fitting) or choosing a more robust minimization (e.g., L1-minimization by iterative re-weighting).

CONCLUSIONS

We have demonstrated a target-oriented joint inversion method, based an iterative least-squares migration/inversion, for imaging incomplete time-lapse seismic data sets. By posing time-lapse imaging as a joint inversion problem, the RJMI method attenuates uncorrected artifacts caused by gaps in the monitor acquisition geometries. We considered an undershoot problem, where obstructions prevent perfect repetition of acquisition geometries for different surveys and a sparse time-lapse data problem, where a random fraction of the monitor data sets are recorded. In both numerical examples, we showed that joint inversion (within the RJMI framework) produces time-lapse images of the best quality relative to migration, normalization with the Hessian diagonal and separate inversion. We recognize that both the separate and joint inversion results can be improved with stronger spatial regularization, but it is arguable that such an approach will introduce too much unjustifiable bias into the inversion. Significant progress made in the field of compressive imaging (Candes and Romberg, 2007) provides a possible pathway for better image recovery from incomplete time-lapse seismic data.

ACKNOWLEDGMENTS

We thank sponsors of the Stanford Exploration Project for their financial support.

REFERENCES

Ajo-Franklin, J. B., J. Urban, and J. M. Harris, 2005, Temporal integration of seismic traveltime tomography: SEG Technical Program Expanded Abstracts, **24**, 2468–2471.

Arogunmati, A. and J. Harris, 2007, Data integration for spatiotemporal imaging: Proceedings, **26**, 2929–2933.

Ayeni, G. and B. Biondi, 2008, Joint wave-equation inversion of time-lapse seismic data: Stanford Exploration Project Report, **136**, 71–96.

Ayeni, G., Y. Tang, and B. Biondi, 2009, Joint preconditioned least-squares inversion of simultaneous source time-lapse seismic data sets: SEG Technical Program Expanded Abstracts, **28**, submitted.

Batzle, M. and Z. Wang, 1992, Seismic properties of pore fluids: Geophysics, **57**, 1396–1408.

Calvert, R., 2005, Insights and methods for 4D reservoir monitoring and characterization: SEG/EAGE DISC (Distinguished Instructor Lecture Course).

Calvert, R. and P. Wills, 2003, The case for 4D monitoring with sparse OBC: EAGE Expanded Abstracts, A15 – A15.

Candes, E. and J. Romberg, 2007, Sparsity and incoherence in compressive sampling: Inverse Problems, **23**, 969–985.

Candes, E. and M. Wakin, 2008, An introduction to compressive sampling: Signal Processing Magazine, IEEE, **25**, 21–30.

Clapp, M. L., 2005, Imaging under salt: illumination compensation by regularized inversion: PhD thesis, Stanford University.

Gray, S. H., 1997, True-amplitude seismic migration: A comparison of three approaches: Geophysics, **62**, 929–936.

Guitton, A., 2004, Amplitude and kinematic corrections of migrated images for nonunitary imaging operators: Geophysics, **69**, 1017–1024.

Hall, S. A., 2006, A methodology for 7D warping and deformation monitoring using time-lapse seismic data: Geophysics, **71**, O21–O31.

Lefeuvre, F., Y. Kerdraon, J. Peliganga, S. Medina, P. Charrier, R. L'Houtellier, and D. Dubucq, 2003, Improved reservoir understanding through rapid and effective 4D: Girassol field, Angola, West Africa: SEG Technical Program Expanded Abstracts, **22**, 1334–1337.

Plessix, R.-E. and W. Mulder, 2004, Frequency-domain finite-frequency amplitude-preserving migration: Geophysical Journal International, **157**, 975–985.

Rickett, J., 2003, Illumination-based normalization for wave-equation depth migration: Geophysics, **68**, 1371–1379.

Rickett, J. E. and D. E. Lumley, 2001, Cross-equalization data processing for time-lapse seismic reservoir monitoring: A case study from the Gulf of Mexico: Geophysics, **66**, 1015–1025.

Shin, C., S. Jang, and D.-J. Min, 2001, Improved amplitude preservation for prestack depth migration by inverse scattering theory: Geophysical Prospecting, **49**, 592–606.

Smit, F., M. Ligtendag, P. Wills, and R. Calvert, 2006, Toward affordable permanent seismic reservoir monitoring using the sparse OBC concept: The Leading Edge, **25**, 454–459.

Symes, W. W., 2008, Approximate linearized inversion by optimal scaling of prestack depth migration: Geophysics, **73**, R23–R35.

Valenciano, A., 2008, Imaging by Wave-Equation Inversion: PhD thesis, Stanford

University.
Versteeg, R., 1994, The Marmousi experience: Velocity model determination on a synthetic complex data set: The Leading Edge, **13**, 927–936.
Whitcombe, D. N., J. M. Marsh, P. J. Clifford, M. Dyce, C. J. S. McKenzie, S. Campbell, A. J. Hill, R. S. Parr, C. Pearse, T. A. Ricketts, C. P. Slater, and O. L. Barkved, 2004, The systematic application of 4D in BP's North-West Europe operations — 5 years on: SEG Technical Program Expanded Abstracts, **23**, 2251–2254.
Zhang, Y., A. Ghodrati, and D. H. Brooks, 2005, An analytical comparison of three spatio-temporal regularization methods for dynamic linear inverse problems in a common statistical framework: Inverse Problems, **21**, 357–382.
Zou, Y., L. R. Bentley, L. R. Lines, and D. Coombe, 2006, Integration of seismic methods with reservoir simulation, Pikes Peak heavy-oil field, Saskatchewan: The Leading Edge, **25**, 764–781.

APPENDIX A

LINEAR LEAST-SQUARES MODELING/INVERSION

From the Born approximation of the linearized acoustic wave equation, the synthetic seismic data d^s recorded by a receiver at $\mathbf{x_r}$ due to a shot at $\mathbf{x_s}$ is given by

$$d^s(\mathbf{x_s}, \mathbf{x_r}, \omega) = \omega^2 \sum_{\mathbf{x}} f_s(\omega) G(\mathbf{x_s}, \mathbf{x}, \omega) G(\mathbf{x}, \mathbf{x_r}, \omega) m(\mathbf{x}), \tag{A-1}$$

where ω is frequency, $m(\mathbf{x})$ is *reflectivity* at image points $\mathbf{x}$, $f_s(\omega)$ is source waveform, and $G(\mathbf{x_s}, \mathbf{x}, \omega)$ and $G(\mathbf{x}, \mathbf{x_r}, \omega)$ are Green's functions from $\mathbf{x_s}$ to $\mathbf{x}$ and from $\mathbf{x}$ to $\mathbf{x_r}$ respectively.

Taking the true recorded data at $\mathbf{x_r}$ to be d^t, the quadratic cost function is given by

$$S(\mathbf{m}) = \|d^s(\mathbf{x_s}, \mathbf{x_r}, \omega) - d^t(\mathbf{x_s}, \mathbf{x_r}, \omega)\|_2^2. \tag{A-2}$$

As shown by previous authors (Plessix and Mulder, 2004; Valenciano, 2008), the gradient $g(x)$ of this cost function (summed over all frequencies, sources and receivers) with respect to reflectivity is the real part of

$$g(\mathbf{x}) = \sum_{w} \omega^2 \sum_{\mathbf{x_s}} \sum_{\mathbf{x_r}} f_s(\omega) G(\mathbf{x_s}, \mathbf{x}, \omega) G(\mathbf{x}, \mathbf{x_r}, \omega) \left(d^s - d^t\right), \tag{A-3}$$

and the Hessian (second derivatives) is the real part of

$$H\left(\mathbf{x}, \mathbf{x}'\right) = \sum_{w} \omega^4 \sum_{\mathbf{x_s}} |f\left(s\right)|^2 G(\mathbf{x_s}, \mathbf{x}, \omega) \bar{G}(\mathbf{x_s}, \mathbf{x}', \omega) \sum_{\mathbf{x_r}} G(\mathbf{x}, \mathbf{x_r}, \omega) \bar{G}(\mathbf{x}', \mathbf{x_r}, \omega), \tag{A-4}$$

where $\mathbf{x}'$ denotes all image points and $\bar{G}$ is the complex conjugate of G. Plessix and Mulder (2004) and Valenciano (2008) discuss this derivation in detail.

Target-oriented Hessian

The large computational cost of full Hessian (equation A-4) makes explicit computation impractical. Previous authors (Shin et al., 2001; Rickett, 2003; Guitton, 2004; Plessix and Mulder, 2004; Valenciano, 2008; Symes, 2008) have discussed possible approximations that reduce the computational cost or remove the need for explicit computation of the full Hessian.

Because reservoirs are limited in extent, the region of interest is usually smaller than the full image space, therefore, the Hessian can be explicitly computed for that region. For our problem, we follow the target-oriented approximation (Valenciano, 2008) to the Hessian, which for a target region $\mathbf{x_T}$ is

$$H\left(\mathbf{x_T}, \mathbf{x_{T+a_x}}\right) = \sum_w \omega^4 \sum_{\mathbf{x_s}} |f(s)|^2 G(\mathbf{x_s}, \mathbf{x_T}, \omega) \bar{G}(\mathbf{x_s}, \mathbf{x_{T+a_x}}, \omega) \sum_{\mathbf{x_r}} G(\mathbf{x_T}, \mathbf{x_r}, \omega) \bar{G}(\mathbf{x_{T+a_x}}, \mathbf{x_r}, \omega), \tag{A-5}$$

where $\mathbf{x_{T+a_x}}$ represents a *small* region around each point within $\mathbf{x_T}$. For any image point, $\mathbf{H}\left(\mathbf{x_T}, \mathbf{x_{T+a_x}}\right)$ represents a row of a sparse Hessian matrix $\mathbf{H}$ whose non-zero components are defined by $\mathbf{a_x}$. The term, $\mathbf{a_x}$, which can be estimated as a function of the decrease in amplitude of the Hessian diagonal, defines the *filter-size* around each image point. Valenciano (2008) discusses the target-oriented Hessian in detail and reviews the computational savings from this approximation.